Extraction of diffusion coefficients from the study of Rb release in different carbon catchers

Julien Guillot, Brigitte Roussière, Pascal Jardin, Emeline Charon, Ugo Forestier-Colleoni, Romain Lafourcade, Martine Mayne-L'hermite, Elie Borg, Vincent Bosquet, François Brisset, et al.

▶ **To cite this version:**

Julien Guillot, Brigitte Roussière, Pascal Jardin, Emeline Charon, Ugo Forestier-Colleoni, et al.. Extraction of diffusion coefficients from the study of Rb release in different carbon catchers. Nuclear Instruments and Methods in Physics Research Section B: Beam Interactions with Materials and Atoms, 2022, 526, pp.9-18. 10.1016/j.nimb.2022.06.005 . cea-03695957

HAL Id: cea-03695957
https://cea.hal.science/cea-03695957

Submitted on 22 Jul 2024

HAL is a multi-disciplinary open access archive for the deposit and dissemination of scientific research documents, whether they are published or not. The documents may come from teaching and research institutions in France or abroad, or from public or private research centers.

L'archive ouverte pluridisciplinaire **HAL**, est destinée au dépôt et à la diffusion de documents scientifiques de niveau recherche, publiés ou non, émanant des établissements d'enseignement et de recherche français ou étrangers, des laboratoires publics ou privés.

Distributed under a Creative Commons Attribution - NonCommercial 4.0 International License

Version of Record: https://www.sciencedirect.com/science/article/pii/S0168583X22001562
Manuscript_e666d323c85322d92cd52b6542324dec

Extraction of diffusion coefficients from the study of Rb release in different carbon catchers

Julien Guillot[a*], Brigitte Roussière[a], Pascal Jardin[b], Emeline Charon[c], Ugo Forestier-Colleoni[c], Romain Lafourcade[c], Martine Mayne-L'Hermite[c], Elie Borg[a], Vincent Bosquet[b], François Brisset[d], Wenling Dong[a], Stéphane Jourdain[a], Matthieu Lebois[ae], Damien Thisse[a]

[a] Université Paris Saclay, CNRS/IN2P3, IJCLab, 91405 Orsay, France

[b] GANIL (Grand Accélérateur National d'Ions Lourds), 14076 Caen Cedex 5, France

[c] Université Paris-Saclay, CEA, CNRS, NIMBE, 91191, Gif sur Yvette Cedex, France

[d] Université Paris Saclay, CNRS, ICMMO, 91405 Orsay, France

[e] Institut Universitaire de France, 1 rue Descartes, 75005 Paris, France

*Corresponding author: julien.guillot@ijclab.in2p3.fr, tel: +33169157248

Keywords: release fraction, carbon nanotubes, graphite, activation energy, diffusion coefficient

---

Abstract:

New Target-Ion Source Systems combining a target and a catcher material are developed in the radioactive beam community, in particular at GANIL, in order to maximise the yield of very short lived atoms by minimizing the atom-to-ion transformation time. The aim of this study is to characterize the release properties of ^{81}Rb collected on two graphite catchers and two carbon nanotube catchers. The release fractions were measured at various catcher-heating temperatures and then compared to the analytical expressions relevant to each catcher. This comparison led to the extraction of the pre-exponential factor (D_0) and the activation energy (E_{act}) involved in the diffusion coefficient of Rb for three carbon microstructures. All these data allowed to define an ideal catcher which could be made of aligned carbon nanotubes of small diameter and oriented in order to collect all the ^{81}Rb atoms produced by the target but also to release them efficiently.

---

1. Introduction

The study of exotic nuclei is fundamental in nuclear physics to improve our knowledge and understanding of nuclear systems. Pushing away the limits of our knowledge requires to produce always more exotic nuclei and thus of shorter half-life. The ongoing research and development program at the SPIRAL1 facility (Système de Production d'Ions Radioactifs Accélérés en Ligne) at GANIL (Grand Accélérateur National d'Ions Lourds) in Caen aims to provide new and intense beams of exotic nuclei [1] using the Isotope Separator On Line (ISOL) method. This method consists in producing radioactive nuclei in a target and stopping them in a matrix, which can be the target material itself or another material, called catcher if separated from the target. Once stopped, the nuclei are neutralized and become atoms. The stopping material is generally maintained at high temperature to accelerate the atomic diffusion out of the material. Once released, atoms effuse to be ionized by an ion source and accelerated by an electric field to form a radioactive ion beam. To maximize the ion intensities, losses during all the atom-to-ion transformation (AIT) process must be minimized. For this, AIT time within the production system must be as short as possible compared to the collected nuclei decay time. This type of Target-Ion Source Systems (TISS) using catcher technology has been studied and developed at IGISOL in Jyväskylä [2] and FRIB at Michigan State University [3].
The new TISS developed at GANIL, called TULIP (Target Ion Source for Short-Lived Isotope Production), combines a target and a catcher material, and aims at minimizing the AIT time by optimizing each step of the

© 2022 published by Elsevier. This manuscript is made available under the CC BY NC user license
https://creativecommons.org/licenses/by-nc/4.0/

AIT process (see ref. [4] for more details on the approach). The first objective of the TULIP project is to produce short-lived alkali isotopes of ^{74}Rb ($T_{1/2}$ = 65 ms). They are produced by fusion-evaporation reactions induced by collision of stable beam at an energy close to the Coulomb barrier with a solid target. The latter is thin enough to allow produced nuclei to pass through. They are then implanted in the first tens of micrometers of the catcher material, depending on its density, and are neutralized. Then Rb atoms released out of the catcher effuse in the TISS cavity and are ionized by surface ionization to form a radioactive ion beam.

Graphite sheet of 200 µm was initially considered as a good candidate for the catcher for technical reasons of resistivity, heat resistance, ease of use, which facilitate the R&D of the TISS, and also for physico-chemical reasons related to its porosity and to the short sticking time of Rb on graphite [5] at the working temperature required for the TISS (~1400°C). Despite mechanical features less adapted to its use in the TULIP TISS design, rigid graphite of 1 µm grains used to design graphite targets of the current FEBIAD and Nanogan TISS at GANIL [6] was also selected for comparison. Two types of carbon nanotubes were also considered owing to their microstructure, i.e. dense tubes separated by large straight regions free of matter, which should favour a rapid effusion of the atoms out of the structure.

The objective of the present work was to determine which catcher material among the four selected offered the fastest release of Rb. The experiment took place at the Tandem accelerator on the ALTO (Accélérateur Linéaire et Tandem à Orsay) platform of Irène Joliot-Curie Laboratory (IJCLab). Our measurement method of the released fractions is an off-line procedure that can only be applied with relatively long-lived isotopes. Thus ^{81}Rb ($T_{1/2}$ = 4.57 h) has been used in the present study. From the results of release versus temperature and with certain assumptions about the microstructure of the material and the implantation depth, pre-exponential factor (D_0) and activation energy (E_{act}) involved in the diffusion coefficient of Rb are extracted. As diffusion properties depend in a negligible way on the isotope of the element, diffusion parameters deduced for ^{81}Rb have been used to evaluate release time and efficiency for ^{74}Rb.

2. Presentation of the catcher materials

The release properties of four carbon samples, potential candidates for the TULIP catcher, were investigated. The catchers studied are two graphite samples that will be hereafter referred to as Papyex®, POCO and two samples of carbon nanotubes aligned either vertically (CNT_v) or horizontally (CNT_h) with respect to the substrate, placed perpendicularly to the ion beam. Figure 1 shows the scanning electron microscopy (SEM) images of the different samples.

All these carbons have different physicochemical characteristics and were characterized when possible by Brunauer, Emmett and Teller (BET) method to determine the specific surface area (SSA) and by helium pycnometry to determine the density and percentage of open and closed porosity.

The Papyex® samples are from a 200 µm thick flexible graphite sheet with anisotropic grain orientation sold by Mersen industry under the name Papyex® (figure 1a). According to the figure 1a, the Papyex® sample is made of very thin sheets of micrometric size in surface and nanometric in thickness. We determined that the material constituting this sample has an apparent density of 1.15 g/cm^3 and has 44 % open porosity and 5 % closed porosity. This sample develops a specific surface area of 22.66 m^2/g.

The graphite samples POCO-ZXF-5Q1 (Entegris, USA) below simply referred to as POCO samples are isomoulded graphite carbon pieces (figure 1b). The samples are 440 µm thick with an apparent density of 1.82 g/cm^3, having respectively 14 % and 5 % of open and closed porosity. This sample has a SSA of 0.72 m^2/g, which corresponds to spherical grains of 3.7 µm in diameter.

The Papyex® and POCO samples were obtained by cutting from the sheets 2 cm by 1.5 cm rectangles suitable for the sample holder.

The CNT_h samples are obtained from sheets composed of carbon nanotubes horizontally aligned (i.e. parallel to the faces of the sheet) and sold by the Merck company (901082-1EA, Merck) as displayed in figure 1c. These

sheets of carbon nanotubes were synthesized according to the protocol developed by Inoue *et al.* [7]. The carbon nanotubes have a SSA of 97.25 m^2/g, an average diameter of 46 nm and a length of 2 mm forming a sheet of about 3 µm thick with an average apparent density of 0.398 g/cm^3. The CNT_h samples correspond to a stack of 4 sheets of horizontally aligned carbon nanotubes representing a mass per unit area of 0.456 $mg/cm^2 \pm 0.024$ mg/cm^2, i.e. a total thickness of about 11.5 µm, deposited on a sheet of Papyex® pre-cut to form rectangles of 2 cm by 1.5 cm.

The CNT_v samples were synthesized and characterised by the NIMBE-LEDNA research team (CEA Paris-Saclay, France). These carbon nanotubes have been synthesized by aerosol-assisted catalytic chemical vapour deposition on a 1.5 cm by 1.5 cm quartz substrate with a thickness of 1 mm [8]–[10]. The carbon nanotubes have a length of 90 µm for an external diameter of 10 nm (figure 1d). The apparent density of this material is 0.3 g/cm^3 and the CNT number density is less than 10^{11} CNT/cm^2. Taking into account the microstructure of the catcher (vertically aligned CNTs which do not form a closed cavity), the part of the catcher not occupied by the CNTs (≥ 92 % of the total surface) can be associated to an open porosity. SSA measurements were not carried out for this catcher because it implied to separate the CNTs from the quartz support, which was not possible due to the small number of samples available.

The physical properties of the four carbon catchers are summarized in Table 1.

3. Measurement of released fractions

The method used to measure the released fractions (*RF*) is adapted from the protocol developed for the research and development on ISOL targets at IJCLab [11], [12]. A copper target (^{65}Cu) 2.72 µm ± 0.29 µm thick was irradiated for 30 minutes with a $^{19}F^{6+}$ beam of 62.5 MeV energy and 20 nAe intensity. ^{81g}Rb and ^{81m}Rb are produced by fusion evaporation and are stopped in a catcher sample located 6 mm behind the target. The target and the catcher sample are placed in a sample holder which allows the adjustment of the ^{19}F beam before bombarding the target. To do so, in addition to the target, a scintillator with a 9.5 mm hole is place in the same sample holder. The latter can be moved perpendicularly to the beam axis. When the scintillator faces the beam, the position, size and shape of the beam are adjusted and when the hole is on the beam axis, the ion beam intensity is measured. The beam has the shape of an ellipse with a 2.30 mm major and a 1.75 mm minor axes. The rate of the isotopes implanted in the catcher was obtained by γ spectrometry measurements: the transitions characteristic of the ^{81}Sr, ^{81m}Rb and ^{81}Rb disintegrations are clearly observed in the spectra recorded with a waiting time between the end of the irradiation and the start of the counting below 45 m and allow us to determine that $(2.2 \pm 0.2)\times10^4$ ^{81}Sr, $(6.6 \pm 0.9)\times10^4$ ^{81m}Rb and $(2.6 \pm 0.4)\times10^4$ ^{81}Rb were implanted per second in the catcher. ^{81}Sr ($T_{1/2}$ = 22.3 m) decaying into ^{81}Rb, it was more advisable to wait for the complete decay of this element before the measurements, *i. e.* about 2h30 (corresponding to ~ 7 times the ^{81}Sr half-life) of waiting after each irradiation. In this way, no ^{81}Rb is created during the heating of the catcher and the release fraction determination is fair. After this waiting time, a first counting of the gamma catcher activity is performed at room temperature for 30 minutes using a germanium detector. At the end of the counting, the catcher is placed under vacuum (10^{-6} mbar) in an oven previously calibrated between 250 °C and 1100 °C, temperature range in which ^{81}Rb released fractions were estimated to be less than 100 %. The temperature of the oven was calibrated using thermocouples and different metals (Sn, Pb, Zn, Al, Cu) heated up to their melting points. The heating device was controlled by a power supply controller, which allowed a repeatability of the heating cycles, in time and power, and of the temperature measurement with ± 20 °C accuracy. After this 30-minute heating step, the catcher residual activity was determined by performing a second gamma spectrometry measurement for 30 minutes.

For each catcher the sample number available, the measurement number performed and the temperature range investigated are presented in Table 2.

Figure 2 shows for the POCO catcher the γ spectra obtained before and after heating at different temperatures. This figure illustrates the influence of temperature on the intensities measured for the 190.5 and 446.1 keV γ transitions resulting from the ^{81g}Rb decay.

The released fraction (*RF*) was obtained from Eq. (1):

$$RF(E_\gamma) = 100 \times \left(1 - \frac{I_{heated}(E_\gamma)}{I_{unheated}(E_\gamma) \times e^{-\lambda . t_w}}\right) \quad (1)$$

with $I_{heated}(E_\gamma)$, the intensity of the γ ray of E_γ energy after heating, $I_{unheated}(E_\gamma)$, the intensity of the γ ray of E_γ energy before heating, λ, decay constant and t_w, waiting time between the first and second counting.

Three RF values were obtained from the γ transitions signing the ^{81g}Rb decay and observed in the γ spectra recorded (190.5, 446.1 and 456.7 keV). The adopted released fraction is the average of these three values weighted by the transition intensities.

4. Results

As shown in table 2, we did not have the same number of samples for each catcher and therefore we could not make the same number of measurements for all the catchers. We had 10 samples of Papyex®, we could make 10 measurements in a wide range of temperature between 250 °C and 965 °C and thus define the temperature range in which graphite releases Rb. For the POCO catcher, 5 measurements were done in a narrower temperature range between 540 °C and 965 °C. For the CNT_v catcher, we had only 3 samples. In order to perform 7 measurements between 310 °C and 940 °C, each sample was irradiated twice with a 48 h delay between the irradiations so that the catcher no longer contained ^{81}Rb atoms ($T_{1/2}$ = 4.5 h). The incident beam was slightly shifted between the two irradiations to avoid ^{81}Rb being implanted in the same place in the catcher and to limit the possible damage caused by the particles entering the catcher. The sample heated to 310 °C did not release any ^{81}Rb, it was used to carry out the measurement at 590 °C without new implantation. The 4 CNT_h samples, made of horizontally-aligned-CNT sheets deposited on a support which is a Papyex®-sheet backing, can be used only once. After the irradiation of the first CNT_h sample, we carried out a γ counting to determine the total amount of ^{81}Rb collected in the catcher. The CNT_h sheets were then separated from the Papyex® backing and the activity emitted by each of two pieces was evaluated by separate gamma spectrometry measurements. We so have determined that 57 % of the ^{81}Rb atoms were stopped in the Papyex® backing and 43 % in the CNT_h sheets. For this catcher, we are interested only by the release from the carbon nanotubes, thus a slightly different protocol has been applied to extract the relevant released fraction. For the three remaining samples, after the irradiation, the first γ counting and the heating, the CNT_h sheets are separated from their Papyex® backing and the second γ counting is performed on the CNT_h sheets alone and on the Papyex® backing separately. The released fractions are obtained by taking for $I_{unheated}$ in Eq. 1 only 43 % and 57 % of the intensity measured during the first counting, respectively. Figure 3 displays all the released fractions measured for the catchers studied during this experiment.

Around 950 °C, all the ^{81}Rb atoms stopped in the Papyex® POCO and CNT_h catchers are released, but for the CNT_v catcher, the released fractions measured do not exceed 69 % (see insert Fig 3). By similarity with the other catchers, we assume that at 943 °C all the ^{81}Rb stopped in the CNT were also released. This implies that the activity still present in the catcher comes from the fraction of ^{81}Rb (31 %) stopped in the quartz and not released at this temperature. As we are only interested by the release from the carbon materials, the released fractions have been normalized to 100 %. Surprisingly, compared to what is observed on the Papyex® catcher, the fractions released from the Papyex® backing are higher at low temperatures and lower at high temperatures. This will be discussed further below.

Taking into account the error bars, it results from Figure 3 that all catchers do not release ^{81}Rb below 551 °C but release almost totally this element above 943 °C. In the temperature range where the release takes place, two categories of catcher seem to emerge. The first group includes the Papyex® and POCO catchers that exhibit very similar released fractions increasing almost linearly in the 590-891 °C temperature range. The second one consists of the two carbon nanotube based catchers, CNT_v and CNT_h, that, compared to the Papyex® and POCO catchers, seem to be better above 771 °C. As it stands and given the low numbers of measurement points and the temperature uncertainty, it seems difficult to identify any impact of the CNT orientation on the release properties of the catcher.

5. Determination of the release time and efficiency

In order to compare the release properties of the studied catchers, release efficiencies are more convenient than released fractions. Both depend on the diffusion coefficient and can be calculated in the frame of models describing diffusion in specific media: in a sheet, a cylinder, a sphere or a fibre [12]–[14]. The choice of the medium in which the diffusion takes place will be made according to the structural properties of the different catchers. In the case of diffusion in a sheet, the profile and depth of implantation must also be known.
Profile and implantation depth were calculated in the frame of the LISE++ software (version 15.13.7) [15]. Then the relevant analytical expressions linking the diffusion coefficient to the released fractions and to the release efficiency for a radioactive isotope are indicated. The method used to extract the activation energy, E_{act}, and the pre-exponential factor, D_0, involved in the diffusion coefficient is described. Finally, the release properties of the catchers are extrapolated and compared at a temperature of 1400 °C, which is the temperature aimed for on-line experiments.

5.1. Implantation depth of ^{81}Rb in the different catchers

The calculations of the implantation require as input parameters the characteristics of the target (nature, thickness), those of the primary beam (energy) and of the catcher (nature, density, thickness). The results of the implantation depth simulations are shown in Figure 4.

The LISE++ simulations indicate that 57 % of the reaction products exit the target. For the graphite catchers, 100 % of the ^{81}Rb leaving the target are stopped and 98 % of them are implanted in the first 8.9 or 5.6 µm of the Papyex® or POCO catcher, respectively. For the CNT_h catcher, 40 % of the ^{81}Rb exiting the target are implanted in the carbon layer of 11.5 µm thick and 0.398 g/cm^3 density and the remaining 60 % in the Papyex® backing. The simulation results are in good agreement with the experimental measurements: 43 % in the CNT_h layers and 57 % in the Papyex® sheet. For the CNT_v catcher, LISE++ indicates that 100 % of the ^{81}Rb are implanted in the CNT_v catcher and 0 % in its quartz support, which is not in agreement with the experimental data (69 %, see section 4). However, the LISE++ code assumes that the materials have a uniformly distributed density, which is not the case for the CNT_v catcher that is architecturally designed with the carbon nanotubes aligned perpendicularly to their support. The ^{81}Rb beam is emitted in a truncated cone with a vertex angle of 74° inside which 34 % of the beam is collinear with the direction of the carbon nanotubes. Under these conditions, taking into account the diameter of the CNT_v and of the Rb atom as well as the number of CNT_v per unit area, only ~ 8 % of the ^{81}Rb have a probability of encountering a carbon nanotube and implanting itself. Combining these two pieces of information, we can conclude that ~ 37 % of the Rb will be stopped in the quartz support. This latter estimate is in rather good agreement with the experimental values, i.e. the CNT_v collects 69 % of the ^{81}Rb and the quartz backing the remaining 31 %. The Rb trapping by quartz was already observed at ISOLDE in our temperature range [16]. Although the LISE++ simulations indicate that the ^{81}Rb atoms are stopped in the catcher, all the available information (catcher architecture, Rb emission angle, quantity deposited in the quartz substrate) leads us to believe that Rb is also implanted in the region between 33.8 and 90 µm. As the catcher architecture is not taken into account by LISE++, the analysis was carried out for these two extreme implantation depths (δ_1 = 33.8 µm and δ_2 = 90 µm). Table 3 presents the results obtained by LISE++ and used for further analyses.

5.2. Diffusion models used

The physicochemical (density, porosity) and structural characteristics (given by the SEM images) lead to the breakdown of the catchers into two groups. The first group includes catchers with a very compact sheet or grain structure, a "high" density (> 1 g/cm^3) and porosity including closed porosity. The second group comprises catchers showing a highly aligned fibre structure, a "low" density (< 0.4 g/cm^3) and with the additional characteristic that the tubes are separated from each other and therefore form neither open nor closed porosity.
These very marked differences between the two classes suggest that the relative weights of diffusion and effusion processes will not be the same in the two cases. The released fractions measured include all the phenomena occurring in the catchers, the diffusion in the material (carbon) and the effusion in the porosity. But,

whatever the microstructure considered (sheet, fibre, cylinder, sphere) and the propagation process (diffusion in material or effusion between the micro-structure of material), the released fractions are analysed using a formalism generally used for diffusion. If the microstructure of the carbons that make up the catchers is not taken into account, the catchers can be analysed globally and assimilated to a sheet of the catcher dimensions. The model of diffusion in a sheet proposed by Fujioka and Arai [13] cannot be used here because the authors assume that, at t = 0, the atoms that will diffuse are uniformly distributed in the sheet and can exit by the two faces of the sheet. For the Papyex® and POCO catchers, the LISE++ calculations showed that the Rb atoms were stopped and distributed in the first µm of the catcher as shown in Figure 4. In the case of CNT catchers, the experiment has shown that Rb are implanted not only along the CNT thickness but also in the Papyex® or quartz support. In the case of the CNT_v, the quartz has not released the implanted Rb and forms a barrier for the Rb implanted in the CNT which can only exit through the free face. In the case of the CNT_h catcher, the Papyex® support has released the implanted Rb but the release profile is very different from that of the Papyex® catcher (figure 3) indicating that there is an exchange between the Papyex® support and the CNT_h. A sheet model with a homogeneous implantation and an exit by only one face is not sufficient to describe the process involved in the CNT_h catcher. Therefore, this catcher will not be considered in the rest of the study.

We have established the relation allowing us to calculate the released fraction and the release efficiency of a radioactive isotope in both cases: diffusion in a sheet with homogeneous implantation in surface and exit by one or two faces.

5.2.1. Relation between released fractions, release efficiencies and diffusion coefficients

The diffusion coefficient (D) is described by an Arrhenius-type equation and is written as follows (equation 2):

$$D = D_0 \, exp\left(-\frac{E_{act}}{kT}\right) \qquad (2)$$

with D_0 the pre-exponential factor, E_{act} the activation energy, T the temperature and k the Boltzmann constant.

5.2.2. Diffusion in a sheet with exit by one or two faces

The analytical expressions for the released fraction and the release efficiency of a radioactive isotope were established following the method of separation of variables described by Crank [17]. The boundary conditions were chosen to describe the experimental conditions.
In the case of an implantation near the surface and exit by two faces, boundary conditions were: at t = 0 the amount of atoms implanted is uniform between 0 and δ and for t > 0, the amount of atoms is zero at positions 0 and d. d is the target thickness and δ the implantation depth. This latter boundary condition means that the diffusing atom, having arrived at the foil surfaces, is released very quickly.
In the case of exit by one face, boundary conditions are: at $t = 0$ the amount of atoms implanted is uniform between 0 and δ the implantation depth ($C(x) = C_0$ for $0 < x < \delta$) and for $t > 0$, the amount of atoms is zero at position 0 indicating that the atoms exit through the face $x = 0$ ($C(0) = 0$) and the condition to be satisfied at the impermeable boundary at the position $x = d$ is $\frac{\partial C}{\partial x} = 0$, d being the thickness of the catcher.
The released fraction during a heating time t_h is written (equation 3):

$$RF(t_h) = 1 - \frac{\sum_{m=1}^{\infty} \frac{1}{(2m-1)^2}\left(1 - \cos\frac{(2m-1)\pi\delta}{\alpha d}\right)\exp\left(-\frac{(2m-1)^2\pi^2 D t_h}{(\alpha d)^2}\right)}{\sum_{m=1}^{\infty} \frac{1}{(2m-1)^2}\left(1 - \cos\frac{(2m-1)\pi\delta}{\alpha d}\right)} \qquad (3)$$

with D the diffusion coefficient, d the target thickness and δ the implantation depth. α is a dimensionless coefficient equal to 1 in case of exit by two faces and equal to 2 in case of exit by one face.

The release efficiency (ε_{RF}) of a radioactive isotope is written (equation 4):

$$\varepsilon_{RF}(\lambda) = \frac{\sum_{m=1}^{\infty} \frac{\pi^2 D}{(2m-1)^2\pi^2 D + \lambda(\alpha d)^2}\left(1 - \cos\frac{(2m-1)\pi\delta}{\alpha d}\right)}{\sum_{m=1}^{\infty} \frac{1}{(2m-1)^2}\left(1 - \cos\frac{(2m-1)\pi\delta}{\alpha d}\right)} \qquad (4)$$

with λ the radioactive constant of the isotope considered.

The d and δ values used for the calculations are indicated in Table 3. Like in Fujioka and Arai's article [10], the foil dimensions other than thickness are assumed to be infinite. Indeed, given the dimensions of the catchers and the implantation profiles obtained with LISE++, almost all atoms will diffuse and exit through the faces perpendicular to the primary beam direction.

5.3. Determination of the constants D_0 and E_{act}

Knowing the characteristics of the sample studied (thickness of the sheet and depth of implantation) and the chosen diffusion model, the change in *RF* as a function of *D* is calculated. From this curve, a value D_{exp} is assigned to each experimental value of *RF*. The parameters E_{act} and D_0 are obtained from D_{exp} values by performing a linear regression using the relation $Ln(D_{exp}) = Ln(D_0) - E_{act}/kT$. Finally, the experimental points RF_{exp} and the calculated curve $RF_{calc}(E_{act}, D_0)$ are plotted as a function of temperature. As can be seen in Figure 3, for the three catchers, no release is observed below 550 °C and full release is obtained above 950 °C. It is just in this temperature range that the linear behaviour of $Ln(D_{exp})$ as a function of $1/T$ is observed. Therefore, fits were performed including only the experimental points verifying this linear behaviour.
It is worth noting that for a given value of *D*, the variables D_0 and E_{act} are not independent (figure 5).

For each catcher various pairs of (E_{act}, D_0) give the same fit of the experimental RF values, for example:
- for POCO: (1.88 eV, 0.14 cm^2/s), (2.18 eV, 4.1 cm^2/s) and (2.48 eV, 100 cm^2/s)
- for Papyex®: (2.04 eV, 2.01 cm^2/s), (2.24 eV, 15.6 cm^2/s) and (2.44 eV, 116 cm^2/s)
- for CNT_v (δ_1 = 33.8 µm): (2.30 eV, 0.025×10^5 cm^2/s), (2.68 eV, 1.84×10^5 cm^2/s) and (3.06 eV, 155×10^5 cm^2/s)
- for CNT_v (δ_2 = 90 µm): (2.10 eV, 0.58×10^3 cm^2/s), (2.30 eV, 5.9×10^3 cm^2/s) and (2.50 eV, 61×10^3 cm^2/s)

It is worth noting that the variation of D_0 as a function of E_{act} is very fast (fig. 5). For the CNT_v catcher analyzed with δ_1 = 33.8 µm, the E_{act} range is higher than for the other catchers leading to a very large D_0 range, spreading over 3 orders of magnitude. The envelope drawn around the $D_0 = f(E_{act})$ curve shows the D_0 variation associated with a given E_{act} value allowing to keep the calculated *RF* values within the experimental error bars (represented on Figure 3). Table 4 shows, for each catcher, the diffusion model used, the E_{act} mean value and the D_0 associated with its error bar.

Figure 6 shows for each catcher the comparison between the experimental released fractions (red dots) and the values calculated using the D_0 and E_{act} parameters reported in Table 4 (blue dotted lines).

It results from table 4 and figure 5 that the E_{act} values are close for the three catchers and are compatible within error bars. The lower the density of the catchers, the greater the D_0 values. These remarks suggest that the activation energy, mainly related to the barrier the atoms have to overcome in the material, does not change from one catcher to the other as all are based on the same atomic bond, and thus slightly depends on the density or on the space free of carbon matter. *A contrario*, the evolution of D_0 versus density suggests that D_0 is mainly related to the microstructure of the catchers free of carbon material (the density of the material associated with an open porosity ≥ 92 % for the CNT_v and equal to 44 % and 14 % for Papyex® and POCO respectively).

6. Estimates of the catcher release efficiencies

As the temperature of the TULIP-TISS is expected to be 1400 °C during on-line experiments, the diffusion coefficients of the different catchers have been extrapolated to this temperature assuming that the D_0 and E_{act} values determined in the 550-950 °C range can still be used at 1400 °C. The diffusion coefficients, the time required for half of the stable nuclei present at t = 0 to be released (t_{50}) and the release efficiency of ^{74}Rb ($\varepsilon_R(^{74}Rb)$) with half-life $T_{1/2}$ = 65 ms calculated at T = 1000 °C and extrapolated at T = 1400 °C are presented in

Table 5.

For all catcher types, when the temperature increases from 1000 to 1400 °C, the diffusion coefficient increases by two orders of magnitude, t_{50} decreases by two orders of magnitude and the ^{74}Rb release efficiency increases by a factor of ~10. Although the diffusion coefficient is greater for Papyex® than for POCO, the t_{50} and the release efficiencies are practically the same. In particular, the calculated release efficiencies at 1400 °C for ^{74}Rb are in the order of 40-50 %.

This similarity may seem surprising at first sight. The SSA of Papyex® (22.66 m^2/g) is greater than that of POCO (0.72 m^2/g), reflecting a finer-grained microstructure, which should lead to a greater diffusion efficiency since the diffusion efficiency is inversely proportional to the grain size [13]. Moreover, the porosity of Papyex® (44 %) is high compared to that of POCO (14 %) and corresponds to a lower density (1.15 g/cm^3 for Papyex® and 1.82 g/cm^3 for POCO). The Rb atoms are therefore implanted more deeply in Papyex® than in POCO (see Figure 4), enlarging their effusion time out of Papyex®. As the effusion efficiency is inversely proportional to the effusion time [18], a greater effusion efficiency is expected in POCO than in Papyex®. The similarity between the calculated release efficiencies of ^{74}Rb out of Papyex® and POCO materials thus probably results from a different time sharing between the diffusion and effusion processes, i.e. a shorter diffusion time but larger effusion time in Papyex® than in POCO.

The CNT_v catcher has more pronounced differences in its structural features governing either the diffusion or the effusion process. In the first case, the size of the tubes is nanometric (10 nm in diameter) and in the second case the porosity is very high (≥ 92 %) and the density very low (0.3 g/cm^3) which leads to an implantation over the whole thickness of the catcher. One can wonder how these properties will interact in the release process and whether one of the components (diffusion or effusion) will be predominant in the overall process. To answer this question,the analysis of the CNT_v released fractions was performed using as model the diffusion in a cylinder [12], [14] with the same radius and length as the CNTs making up the carpet (R = 5 nm and L = 90 µm). Choosing this model means that the release of the atoms out of the catcher is only governed by the diffusion out of the cylinder material, and that the contribution of the effusion between the cylinders is negligible. In other words, the Rb atom is considered to leave the catcher when it leaves the tube. The figure 7 and the table 6 show the result of this analysis.

The comparison between figures 6 and 7 shows that, for the CNT_v catcher, the experimental RF value are reproduced as well by the sheet model as by the cylinder model. The comparison between the activation energies and D_0 obtained using either the catcher-sized sheet model or the carbon nanotube-sized cylinder model shows that the activation energies are close (2.68 and 2.3 eV or 2.42 eV) as expected as the carbon bonds are identical, and that $\sqrt{D_0}$ is reduced by a factor of 8.3×10^4 or 1.5×10^4 depending on the implantation depth assumed (33.8 or 90 µm respectively). These factors are close to the value expected (1.8×10^4) considering the thickness of matter (or matter + free space) traversed, 90 µm in the case of the sheet and 5 nm in the case of the cylinder; the maximum remaining factor (4.6) results from the small difference between the activation energies found in the sheet and cylinder analyses and the strong dependence of D_0 on E_{act} (see figure 5).

The values of t_{50} and $\varepsilon_R(^{74}Rb)$ obtained at 1000 and 1400 °C using the sheet model in the extreme implantation conditions (δ = 33.8 and 90 µm) frame those calculated with the cylinder model (see tables 5 and 6). This shows that for the CNT_v catcher, the release is mainly governed by diffusion in the CNT and that effusion plays a minor role.

It should be remembered that, as only 69 % of the Rb were stopped in the CNT_v, the effective release efficiency of this catcher is 56.6 % according to the cylinder model. If the CNTs had grown not on the quartz backing but on a releasing support, Rb diffusion could occur at the boundary between both media (CNTs and support). This diffusion rate depends on the diffusion coefficients in both media and on the size of the contact area between the CNTs and the support. The vertically aligned CNTs occupy only 8 % of the support surface, a contact area assumed lower than in the CNT_h-catcher case. The diffusion of Rb between the CNTs and the support would be minimised compared to what was observed with the CNT_h catcher and the release efficiency of the support

would be added to that of the CNTs in proportion to the atoms collected in the support. For example, if the CNT_v had grown on a Papyex® support, the overall release efficiency for ^{74}Rb at 1400 °C would be 71 %.

7. Conclusion

We studied the release profile of ^{81}Rb out of four catchers (Papyex®, POCO, CNT_v and CNT_h) with different microstructures in a temperature range from 250 °C to 950 °C. Two categories of release emerged, related to Papyex® and POCO materials on the one hand and CNT_h and CNT_v on the other.

The analysis of these release profiles was carried out in the framework of a diffusion model in a catcher-sized sheet. In order to carry out this analysis, the profile and the depth of the collected atoms were obtained using the LISE++ calculation code. In all the materials, the implantation was considered uniform.

In the case of CNT_v and CNT_h catchers, part of the atoms was collected in the support (quartz and Papyex® respectively). The release profile of the CNT_v catchers showed that the atoms implanted in the quartz support were not released. In the case of the CNT_h catchers, the profiles of the released fractions obtained for the Papyex® support on the one hand and for the CNT_h on the other hand suggest an exchange of ^{81}Rb between these two materials during the release, making the analysis of this catcher hazardous as the models used are diffusion in a sheet with release from one or two faces. Neither of them can describe an exchange between two materials.

For the other three catchers (Papyex®, POCO and CNT_v) the results of the analysis were used to extrapolate the release properties of ^{74}Rb at 1400 °C (the temperature aimed for the TULIP TISS). In the case of graphite catchers, the implantation occurred in the first micrometers (8.9 µm for Papyex® and 5.6 µm for POCO). The release efficiencies at 1400°C for ^{74}Rb were estimated to be 47 % and 48 % for the Papyex® and POCO catchers respectively. Despite the differences in microstructure (SSA, porosity, and thus density) between Papyex® and POCO, which necessarily lead to different contributions of effusion and diffusion in these two catchers, release efficiencies are similar showing a compensation between both release processes. The best release efficiency was obtained for the CNT_v catcher (estimated at 82 % for ^{74}Rb at 1400 °C). This catcher has a very high porosity ($\geq$ 92 %). The diffusion plays a dominant role in the release process as shown by the double analysis performed in the framework of the sheet and cylinder models. In conclusion, carbon nanotube catcher (CNT_v) has very promising release properties due to its architecture. Once out of the tube by diffusion, the effusion time up to be out of the catcher can be neglected because the carbon nanotubes are aligned toward the outer surface of the catcher and the free space between the tubes is important, thus the tubes form no closed porosity. Therefore, an ideal catcher could consist of carbon nanotubes having a small diameter to minimize the diffusion and long enough and tilted to stop the nuclei.

Acknowledgements

This work is part of the TULIP project (Projet-ANR-18-CE31-0023) supported by the French National Agency of Research (ANR). The authors would like to thank the ALTO team and Sébastien Wurth (SPR team leader) for help in the implementation of the experimental devices and for the beam preparation.

References:

[1] P. Jardin *et al.*, 'New target ion source systems at GANIL/SPIRAL1: Prospective', *Nucl. Instrum. Methods Phys. Res. Sect. B Beam Interact. Mater. At.*, vol. 376, pp. 64–67, Jun. 2016, doi: 10.1016/j.nimb.2016.03.020.

[2] T. Kessler, I. D. Moore, H. Penttilä, F. Quinquis, and J. Äystö, 'Towards on-line production of N=Z ^{94}Ag at IGISOL', *Nucl. Instrum. Methods Phys. Res. Sect. B Beam Interact. Mater. At.*, vol. 266, no. 19, pp. 4420–4424, Oct. 2008, doi: 10.1016/j.nimb.2008.05.030.

[3] Y. Liu and M. S. Smith, 'Computational Studies of Solid Stoppers for Generating Intense Exotic Radioactive Ion Beams at FRIB', Oak Ridge National Lab. (ORNL), Oak Ridge, TN (United States), ORNL/TM-2018/839, Oct. 2018. doi: 10.2172/1484136.

[4] V. Kuchi *et al.*, 'High efficiency ISOL system to produce neutron deficient short-lived alkali RIBs on GANIL/SPIRAL 1 facility', *Nucl. Instrum. Methods Phys. Res. Sect. B Beam Interact. Mater. At.*, vol. 463, pp. 163–168, Jan. 2020, doi: 10.1016/j.nimb.2019.05.070.

[5] A. Pichard, 'Développement de faisceaux d'ions radioactifs pour le projet SPIRAL 2', Thesis, Caen, 2010. Accessed: Sep. 10, 2021. [Online]. Available: http://theses.fr/2010CAEN2052

[6] P. Delahaye *et al.*, 'New exotic beams from the SPIRAL 1 upgrade', *Nucl. Instrum. Methods Phys. Res. Sect. B Beam Interact. Mater. At.*, vol. 463, pp. 339–344, Jan. 2020, doi: 10.1016/j.nimb.2019.04.063.

[7] Y. Inoue *et al.*, 'Anisotropic carbon nanotube papers fabricated from multiwalled carbon nanotube webs', *Carbon*, vol. 49, no. 7, pp. 2437–2443, Jun. 2011, doi: 10.1016/j.carbon.2011.02.010.

[8] M. Pinault, M. Mayne-L'Hermite, C. Reynaud, V. Pichot, P. Launois, and D. Ballutaud, 'Growth of multiwalled carbon nanotubes during the initial stages of aerosol-assisted CCVD', *Carbon*, vol. 43, no. 14, pp. 2968–2976, Nov. 2005, doi: 10.1016/j.carbon.2005.06.011.

[9] C. Castro, M. Pinault, D. Porterat, C. Reynaud, and M. Mayne-L'Hermite, 'The role of hydrogen in the aerosol-assisted chemical vapor deposition process in producing thin and densely packed vertically aligned carbon nanotubes', *Carbon*, vol. 61, pp. 585–594, Sep. 2013, doi: 10.1016/j.carbon.2013.05.040.

[10] E. Charon, M. Pinault, M. Mayne-L'Hermite, and C. Reynaud, 'One-step synthesis of highly pure and well-crystallized vertically aligned carbon nanotubes', *Carbon*, vol. 173, pp. 758–768, Mar. 2021, doi: 10.1016/j.carbon.2020.10.056.

[11] B. Hy *et al.*, 'An off-line method to characterize the fission product release from uranium carbide-target prototypes developed for SPIRAL2 project', *Nucl. Instrum. Methods Phys. Res. Sect. B Beam Interact. Mater. At.*, vol. 288, pp. 34–41, Oct. 2012, doi: 10.1016/j.nimb.2012.04.031.

[12] J. Guillot *et al.*, 'Development of radioactive beams at ALTO: Part 2. Influence of the UC_x target microstructure on the release properties of fission products', *Nucl. Instrum. Methods Phys. Res. Sect. B Beam Interact. Mater. At.*, vol. 440, pp. 1–10, Feb. 2019, doi: 10.1016/j.nimb.2018.11.039.

[13] M. Fujioka and Y. Arai, 'Diffusion of radioisotopes from solids in the form of foils, fibers and particles', *Nucl. Instrum. Methods Phys. Res.*, vol. 186, no. 1, pp. 409–412, Jul. 1981, doi: 10.1016/0029-554X(81)90933-2.

[14] J. Guillot, B. Roussière, S. Tusseau-Nenez, D. S. Grebenkov, and M. Ignacio, 'Influence of density and release properties of UC_x targets on the fission product yields at ALTO', *Nucl. Instrum. Methods Phys. Res. Sect. B Beam Interact. Mater. At.*, vol. 468, pp. 1–7, Apr. 2020, doi: 10.1016/j.nimb.2020.02.016.

[15] O. B. Tarasov and D. Bazin, 'LISE++: Radioactive beam production with in-flight separators', *Nucl. Instrum. Methods Phys. Res. Sect. B Beam Interact. Mater. At.*, vol. 266, no. 19, pp. 4657–4664, Oct. 2008, doi: 10.1016/j.nimb.2008.05.110.

[16] E. Bouquerel *et al.*, 'Purification of a Zn radioactive ion beam by alkali suppression in a quartz line target prototype', *Eur. Phys. J. Spec. Top.*, vol. 150, no. 1, pp. 277–280, Nov. 2007, doi: 10.1140/epjst/e2007-00323-4.

[17] J. Crank, *The mathematics of diffusion*, 2nd edition. Oxford: Clarendon Press, 1975.

[18] R. Kirchner, 'On the release and ionization efficiency of catcher-ion-source systems in isotope separation on-line', *Nucl. Instrum. Methods Phys. Res. Sect. B Beam Interact. Mater. At.*, vol. 70, no. 1, pp. 186–199, Aug. 1992, doi: 10.1016/0168-583X(92)95930-P.

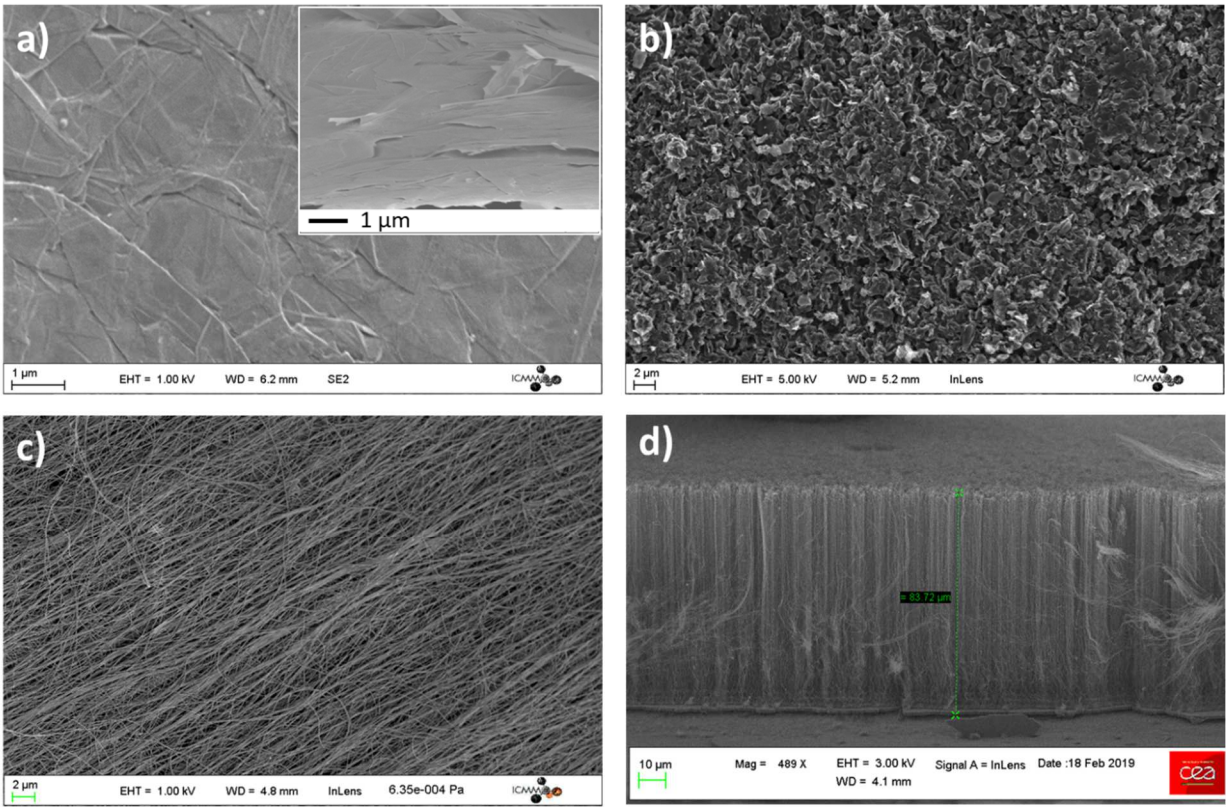

Figure 1 : SEM images of the catchers used in this experiment
a) Papyex® b) POCO c) Carbon nanotubes aligned horizontally (CNT_h) d) Carbon nanotube aligned vertically (CNT_v).

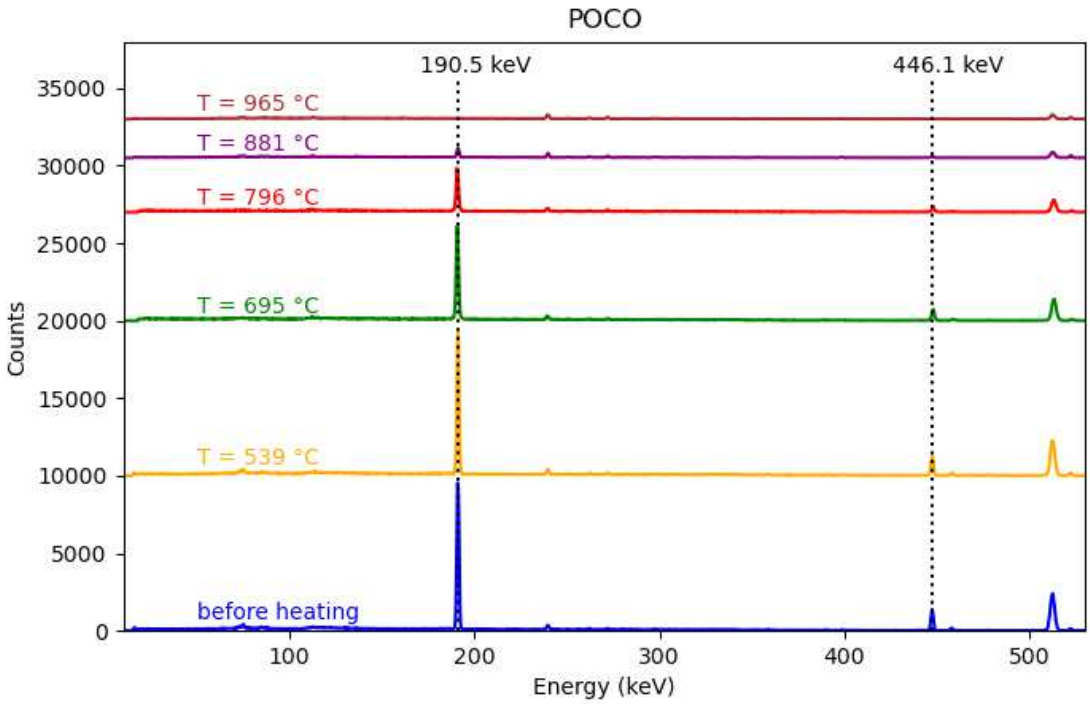

Figure 2: Spectra obtained by γ spectrometry before and after heating for different temperatures for POCO samples. An arbitrary constant was added to the heated spectra in order to obtain a more understandable figure.

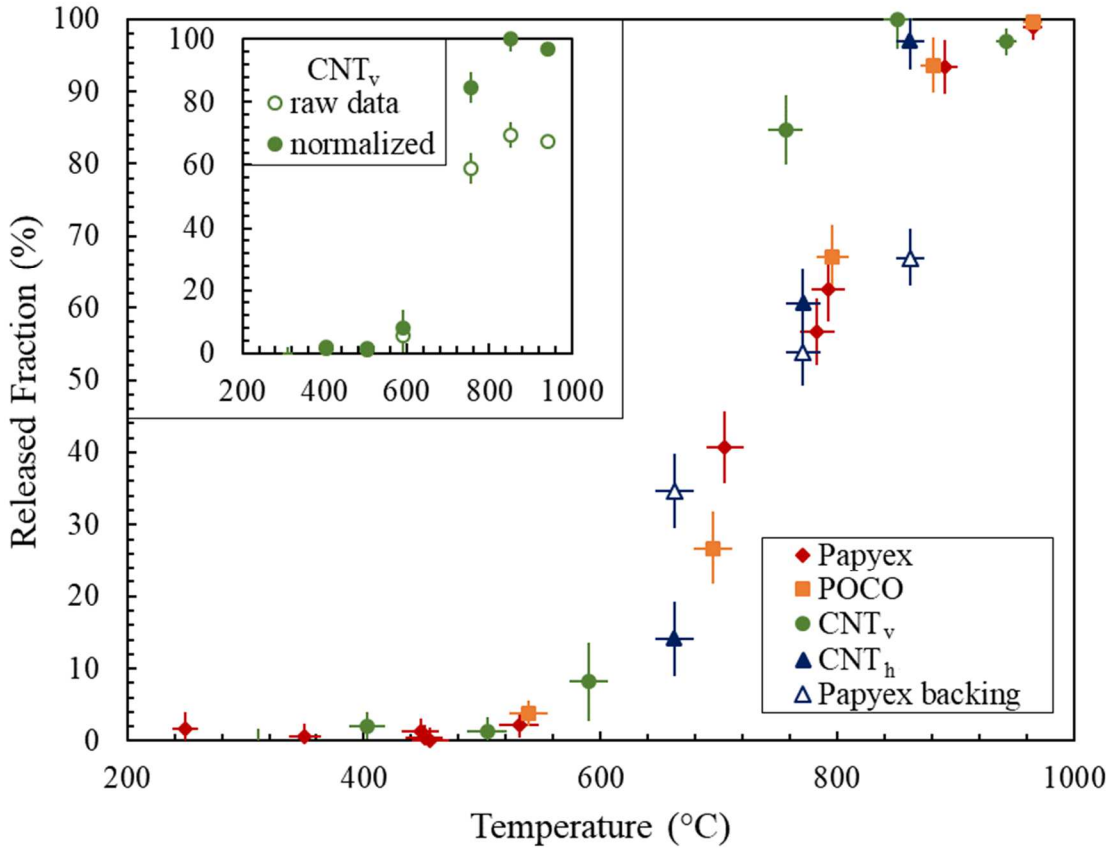

Figure 3: Released fractions measured for the catchers studied in this experiment. For the CNT_v, the raw and normalized data (see text) are presented in the insert.

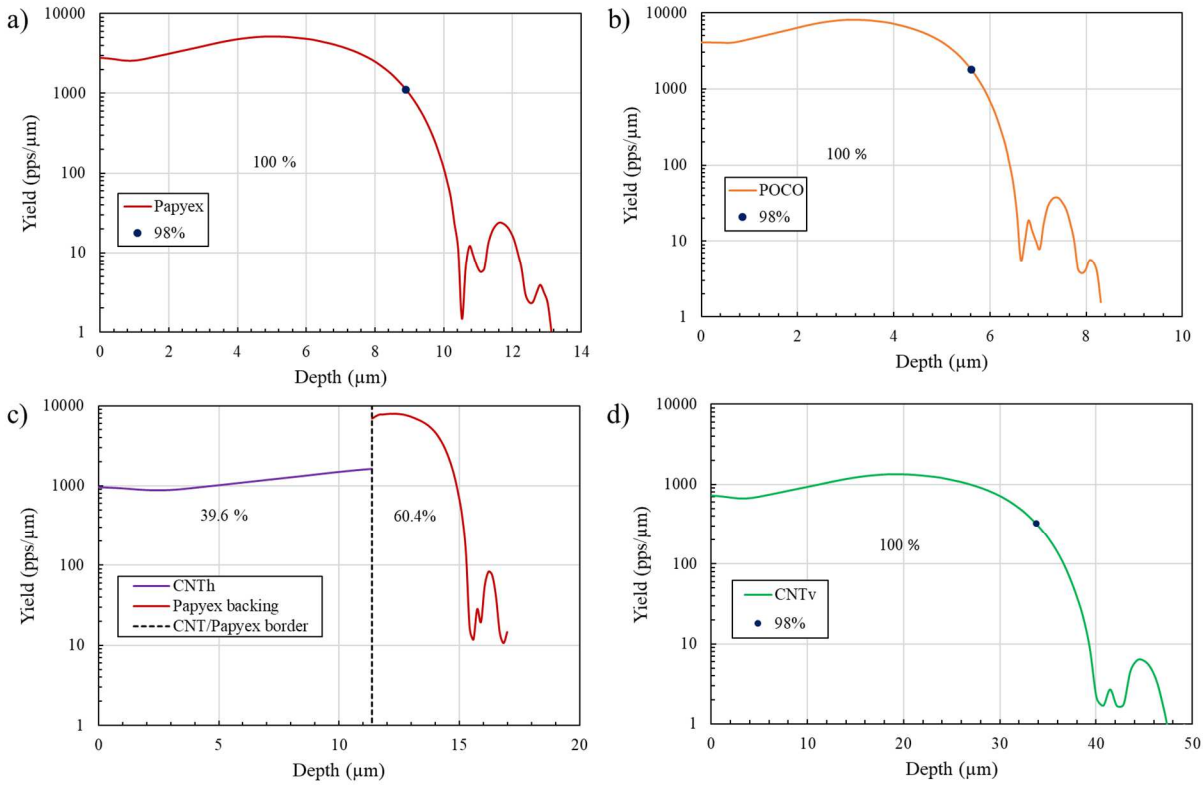

Figure 4: LISE ++ simulations of the Rb implantation depth in catchers with different densities

a) Papyex® b) POCO c) CNT_h d) CNT_v

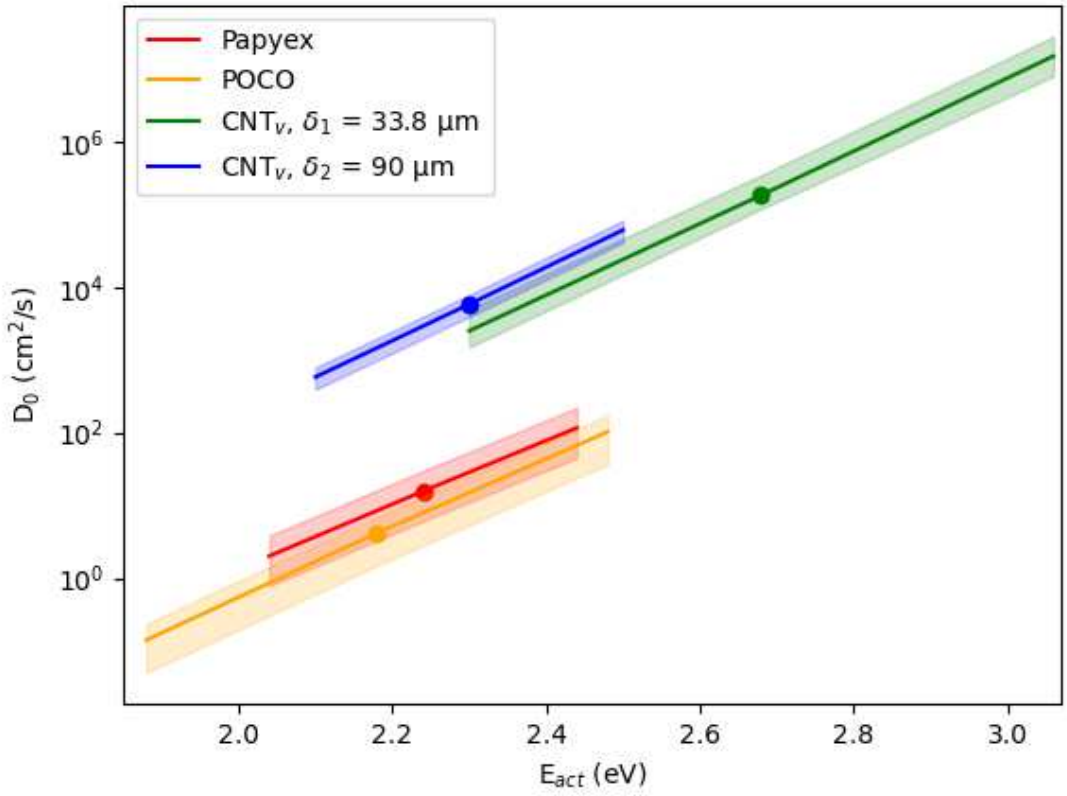

Figure 5: Variation of D_0 as a function of E_{act} for Papyex®, POCO and CNT_v catchers. For the CNT_v catcher, the result obtained with the two analyses (δ_1 = 33.8 µm and δ_2 = 90 µm) are plotted. The dots represent the E_{act} mean values with the associated D_0 taken in the rest of the study.

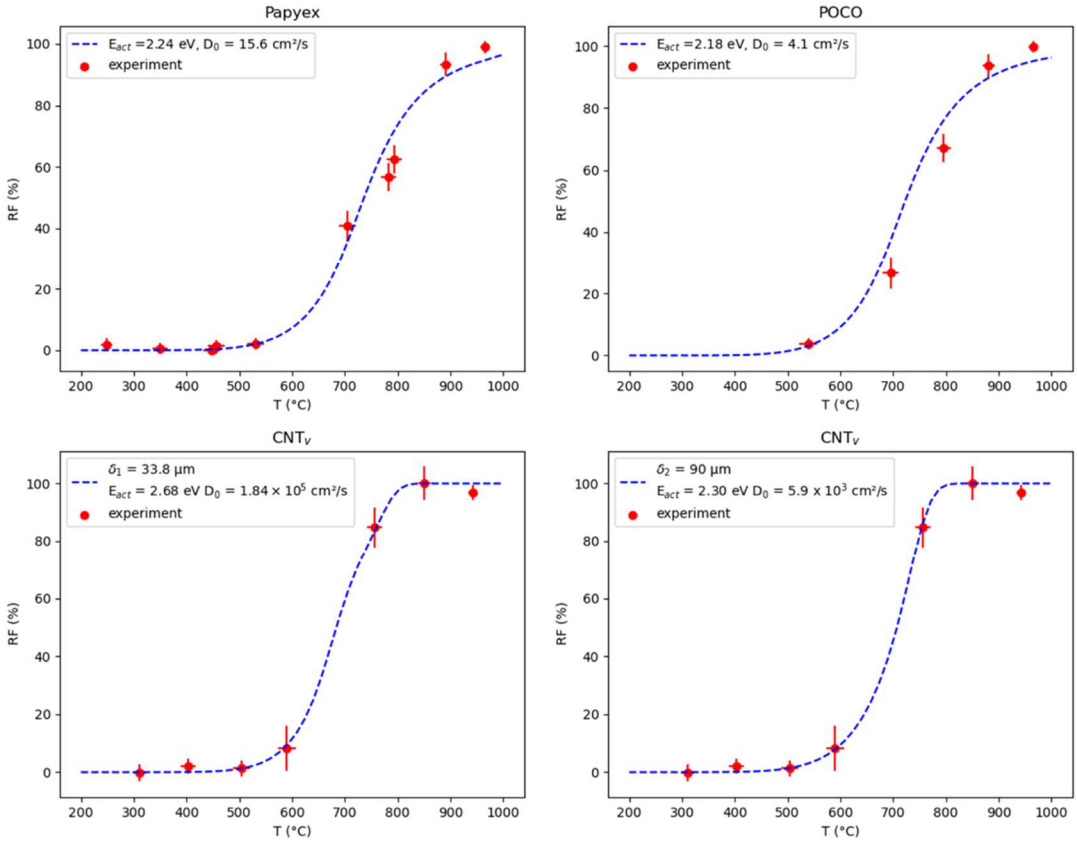

Figure 6: Comparison between the values of the experimental (red dots) and calculated (blue dotted lines) released fractions.

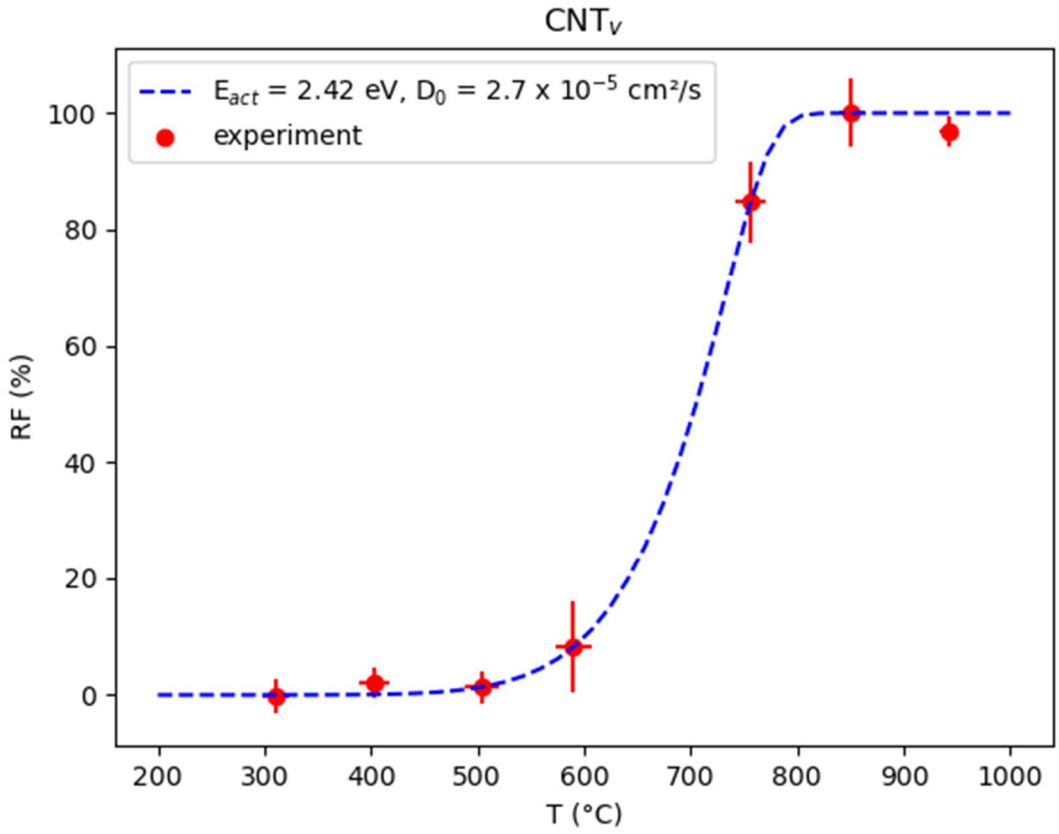

Figure 7: Comparison between the values of the experimental (red dots) and calculated (blue dotted lines) released fractions for the CNT_v catcher. The calculated values are obtained with D_0 and E_{act} given by the cylinder analysis.

Table 1: Physical properties of the four carbon catchers; in the third column, L, l and d indicate the length, width and thickness of the catcher

Catcher	Substrate	Catcher dimension	Density (g/cm^3)	Porosities (%)		SSA (m^2/g)	CNT properties		
		L (cm) × l (cm) × d (µm)		open	close		Diameter	Length	Number
Papyex®	-	2 × 1.5 × 200	1.15	44	5	22.66	-	-	-
POCO	-	2 × 1.5 × 440	1.82	14	5	0.72	-	-	-
CNT_h	Papyex®	2 × 1.5 × 11.5	0.398	-	-	97.25	46 nm	2 mm	-
CNT_v	Quartz	1.5 ×1.5 × 90	0.3	92*	-	-	10 nm	90 µm	$< 10^{11}$ cm^{-2}

* part of the catcher not occupied by the CNTs

Table 2: For each catcher, number of samples and of measurement points and temperature range studied

Catcher	Carbon source	Number of samples	Number of measurements	Temperature range
Papyex®	Graphite	10	10	250 °C – 965 °C
POCO	Graphite	5	5	540 °C – 965 °C
CNT_v	Carbon nanotube	3	7	310 °C – 940 °C
CNT_h	Carbon nanotube	4	3	660 °C – 860 °C

Table 3: Results of implantation of Rb obtained with the LISE++ simulation code. In the third column, the thickness calculated by LISE ++ and required to stop 98 % of the Rb produced is given. The fourth column gives the thickness of the catchers used. The fifth column gives the actual thickness of the material studied in which the Rb is stopped.

Catcher	Density (g/cm^3)	Implantation depth (µm)	Catcher thickness "d" (µm)	Real implantation depth "δ" (µm)
Papyex®	1.15	8.9	200	8.9
POCO	1.82	5.6	440	5.6
CNT_h	0.398	25.4	11.5 (CNT_h) + 200 (Papyex® backing)	11.5
CNT_v	0.3	33.8	90 (CNT_v) + 1000 (Quartz support)	33.8 (δ_1) 90 (δ_2)

Table 4: D_0 and E_{act} values determined for each catcher within the temperature range of 550 °C to 950 °C

Catcher	Density (g/cm^3)	Model	Parameters	D_0 (cm^2/s)	E_{act} (eV)
POCO	1.82	Sheet with exit by two faces	δ = 5.6 µm d = 200 µm	4.1 ± 2.8	2.18
Papyex®	1.15	Sheet with exit by two faces	δ = 8.9µm d = 440 µm	15.6^{+14}_{-10}	2.24
CNT_v	0.3	Sheet with exit by one face	δ_1 = 33.8 µm d = 90 µm	$(1.84\ ^{+1.66}_{-0.64}) \times 10^5$	2.68
			δ_2 = 90 µm d = 90 µm	$(5.9\ ^{+2.1}_{-1.9}) \times 10^3$	2.30

Table 5: Diffusion coefficients (D), time to release 50 % atoms implanted (t_{50}) and ^{74}Rb release efficiency ($\varepsilon_R(^{74}Rb)$) calculated at 1000 °C for the different catchers from the E_{act} and D_0 values obtained during the analysis of the released fractions and extrapolated to a temperature of 1400 °C.

Catcher	T (°C)	D (cm^2/s)	t_{50} (s)	$\varepsilon_R(^{74}Rb)$
POCO E_{act} = 2.18 eV D_0 = 4.1±2.8 cm^2/s	1000	$(9.7 \pm 6.5) \times 10^{-9}$	7.5^{+13}_{-3}	0.05 ± 0.02
	1400	$(1.1 \pm 0.7) \times 10^{-6}$	$0.07^{+0.12}_{-0.03}$	$0.48^{+0.08}_{-0.15}$
Papyex® E_{act} = 2.24 eV $D_0 = 15.6^{+14}_{-10}$ cm^2/s	1000	$(2.1\ ^{+1.9}_{-1.3}) \times 10^{-8}$	$8.7^{+13.5}_{-4.1}$	0.05 ± 0.02
	1400	$(2.8\ ^{+2.6}_{-1.7}) \times 10^{-6}$	$0.07^{+0.10}_{-0.03}$	$0.47^{+0.10}_{-0.14}$
CNT_v (δ = 33.8 µm) E_{act} = 2.68 eV $D_0 = (1.84\ ^{+1.66}_{-0.64}) \times 10^5$ cm^2/s	1000	$(4.5\ ^{+4.1}_{-1.5}) \times 10^{-6}$	0.6 ± 0.3	$0.19^{+0.07}_{-0.03}$
	1400	$(1.6\ ^{+1.4}_{-0.5}) \times 10^{-3}$	$0.0017^{+0.001}_{-0.001}$	0.92 ± 0.03
CNT_v (δ = 90 µm) E_{act} = 2.30 eV $D_0 = (5.9\ ^{+2.1}_{-1.9}) \times 10^3$ cm^2/s	1000	$(4.6\ ^{+1.7}_{-1.5}) \times 10^{-6}$	$3.5^{+1.6}_{-0.9}$	0.07 ± 0.01
	1400	$(6.9\ ^{+2.5}_{-2.2}) \times 10^{-4}$	$0.023^{+0.011}_{-0.007}$	$0.72^{+0.05}_{-0.08}$

Table 6: D_0 and E_{act} values determined for CNT_v catcher within the temperature range of 550 °C to 950 °C in the frame of the cylinder model. Diffusion coefficients (D), time to release 50 % atoms implanted (t_{50}) and ^{74}Rb release efficiency ($\varepsilon_R(^{74}Rb)$) calculated at 1000 °C and extrapolated to a temperature of 1400 °C.

E_{act} (eV)	D_0 (cm^2/s)	T (°C)	D (cm^2/s)	t_{50} (s)	$\varepsilon_R(^{74}Rb)$
2.42	$(2.7 \pm 2.0) \times 10^{-5}$	1000	$(7.1\ ^{+3.6}_{-2.2}) \times 10^{-15}$	$2.2^{+1.3}_{-1.0}$	$0.10^{+0.03}_{-0.02}$
		1400	$(1.4^{+1.0}_{-0.5}) \times 10^{-12}$	$0.011^{+0.007}_{-0.005}$	0.82 ± 0.07